Astronomy & Astrophysics manuscript no. Nicolas
December 5, 2019

Redshift evolution of the SN stretch distribution

N. Nicolas[1], M. Rigault[2], R. Graziani[2], M. Briday[1], Y. Copin[1], and Y. Kim[1]

[1] Université de Lyon, F-69622, Lyon, France; Université de Lyon 1, Villeurbanne; CNRS/IN2P3, Institut de Physique des Deux Infinis, Lyon
[2] Université Clermont Auvergne, CNRS/IN2P3, Laboratoire de Physique de Clermont, F-63000 Clermont-Ferrand, France.

Received 2 November 1992 / Accepted 7 January 1993

ABSTRACT

Context. Type Ia supernovae (SNe Ia) allow for the construction of the Hubble diagram, giving us information about the Universe's expansion and its fondamental components, one of which is dark energy. But systematic uncertainties are now starting to be limiting in our ability to measure those parameters. In particular, the physics of SNe Ia is still mostly unknown, and is thought not to change in time/with the redshift.
Aims. In an attempt to reduce those uncertainties, we try to find an empirical law describing SNe Ia's length of explosion (stretch) evolution with the redshift.
Methods. We started by getting a complete sample representing all of the stretch distribution that Nature can give us, before using LsSFR measurments, an age tracer which evolution with redshift is known, that has been shown to have a strong correlation with the stretch. We compare their AICc, an estimator of the relative quality of statistical models that includes the number of free parameters, to determine which ones describe besto the data.
Results. Models with an evolution of the stretch with the redshift have a better AICc than the ones without.
Conclusions. We find that implementing these models allows us to fit the data better than models without stretch evolution.

Key words. Cosmology – Type Ia Supernova – Systematic uncertainties

1. Introduction

Type Ia supernovae (SNe Ia) are powerful cosmological distance indicators that have enabled the discovery of the acceleration of the Universe's expansion (**??**). They remain today a key comological probe to understand the properties of dark energy (DE) as it is the only tool able to precisely map the recent expansion rate $z < 0.5$, when DE is driving it (e.g. **?**). They also are key to directly measure the Hubble Constant (H_0) provided one can calibrate their absolute magnitude (Riess et al. 2016; Freedman et al. 2019). Interestingly, the value of H_0 derived when the SNeIa are anchored on Cepheids (the SH0ES project **?**Riess et al. 2016) is $\sim 5\,\sigma$ higher than what is predicted by cosmic microwave background (CMB) data measured by Planck assuming the standard ΛCDM or when the SN luminosity is anchored at intermediate redshift by the baryon accoustic oscillation (BAO) scale (Riess et al. 2019; **?**; **?**; **?**). While using the tip of the red giant branch technique in place of the Cepheids seem to favor lower values of H_0 (**??**) time delay measurements from strong lensing seem to also favor high H_0 values (Wong et al. 2019).

The H_0 tension has received a lot of attention as it could be a sign of new fundamental physics. Yet, no simple solution is able to accomodate this H_0 tension when accounting for all other probes and the current most promising scenario appears to be a burst of expansion at the matter-radiation decoupling moment caused by a (fine tuned) early dark energy (**?**).

Alternatively, systematic effects affecting one or several of the aforementioned analysis could also explain the tension. In Rigault et al. (2015) we suggested that SNe Ia from the cepheid calibrator sample differ significantly to the one from the Hubble flow sample that enables to derive H_0. Indeed, Cepheid are very young stars and the existence of Cepheids in a galaxy implies that the host is star forming. In (**?**) we claimed that a more than 90% of the calibrator SNe Ia arise from a young-progenitor propulation while this population only accounts for about half of the Hubble flow sample. Following **?** and (Rigault et al. 2013), we further showed that young and old progenitor SNe Ia have a different magnitude of about 0.15 mag. This has been confirmed for modern standardization technique (SALT2.4 **??**) with high significance ($\sim 6\sigma$) in (Rigault et al. 2018) as well as independently by **?** at $\sim 7\sigma$. As detailed in (**?**), if the magnitude difference between young and old SNe Ia is indeed of 0.15 mag and if SNe Ia from the calibrator sample is fully dominated by young SNeIa, the effect on H_0 of the existance of these two SNe Ia populations is of 3.5%. Accounting for the fact that another environmental effect (the mass-step) is already included in the SH0ES analysis, the net bias in the SH0ES analysis is expected closer to 3% (see table 6 of Rigault et al. 2015).

SHOULD BE SHORTENED A LOT: However, the importance of this astrophysical bias in the direct measurement of H_0 is still highly debated. We also highlight that it could not explain the high value of H_0 derived by strong lensing. First, **?** did not find any environmental bias when extending the (Rigault et al. 2015) study. It was more recently reported in (**?**) that indeed local host analysis has significant influence on the SN magnitude but much more importantly than claimed in (Rigault et al. 2018) and with a connection with the progenitor physics and/or a line of sight effect that is unclear. More importantly, Riess et al. (2016) attended to mimic the cepheid sample selection function on the Hubble flow sample by removing SNe Ia from the latter if they classificed their host as early-type or non-star forming. They measured that doing so has no effect on the measurement of H_0.

This paper is part of a series of papers where we test the validity of the two SNe Ia population models developped in (Rigault et al. 2018).Briday et al. in prep will present how using different environmental tracer is affecting our ability to distinguish the two populations, and Rigault et al. in prep will further study the connection with H_0. Here we analyze predictions concerning the SNe Ia redshift drifts: (1) that the distribution of the SNIa stretch, a purely intrinsic SNIa property, is evolving as a function of redshift and (2) that this population-drift follows the relation that (Rigault et al. 2018) derived assuming that one population is "young" with a rate proportional to the star formation rate in the Universe and the second is "old" with a rate proportional to the stellar mass.

The concept of the SNeIa age dichotomy arised when the SNIa rate has first been studied. **?** have shown that the relative SNe Ia rate in galaxies could only be explained if two populations existed, one young, following the host star formation activity, and one old following the host stellar mass (the so called "prompt and delayed" or "A+B" model). In Rigault et al. (2018) we used the specific star formation rate at the SN location (Local sSFR or LsSFR) to classify which are the prompts (those with a high LsSFR) and which are the delayed (those with low LsSFR). Since the first SNe Ia host analysis, the SN strech has been known to be strongly correlated with the SN host properties (**??**) and it has been extensively confirmed since (e.g. **??**A'; **?**; **?**). Following the "A+B" model and the connection between SN stretch and host properties, (**?**) first discussed the potential redshift drift of the SN strech distribution. In this paper we revisit this analysis with the most recent SNe Ia dataset and we test the validity of the two SNIa age populations model developped by (Rigault et al. 2018).

We present in section **??** the sample we are using for this analysis, which is based on the pantheon dataset (**?**). We discuss the importance of obtaining a "complete" sample, i.e. reprensentative of the true underlying SNe Ia distribution, and how we build one from the Pantheon sample. We then present in section **??** our modeling of the distribution of stretch as a function of redshift based on the relative stretch distrubtion of young and old SNeIa. Our results are presented in section **??** where we test if the distribution of stretch does evolve as a function of redshift and if the age-model is in good agreement with this evolution. We discuss our results and conclude in section **??**.

Throughout the paper we use the Planck 2015 cosmology from the astropy library.

2. Sample

We base our analysis on the latest SNe Ia compilation: the Pantheon catalog from Scolnic et al. (2018). Using this dataset, we aim at probing the evolution of the distribution of SNe Ia stretch in nature as a function of redshift. We thus have to

Because the observed magnitude of a SN Ia is correlated with its stretch and its color, in a magnitude limited survey such as those consituing most of the Pantheon sample, the distribution of these lightcurve parameters is not representative of the true underlying distribution above a certain limiting redshift. The first SNe Ia that such a survey will miss because they will be too faint are indeed the reddest and the lowest-stretch SNe Ia. If such a selection effect is not accounted for, we might confuse true population drift we selection function or conversally.

The figure 1 shows the distribution of stretch for the magnitude limited samples of the Pantheon data, i.e. PanStarrs (PS1 **?**), the Sloan Digital Sky Survey (SDSS **?**) and the SuperNovae Legacy Survey (SNLS **?**). An ellipse in the salt2.4 (x_1, c) plan

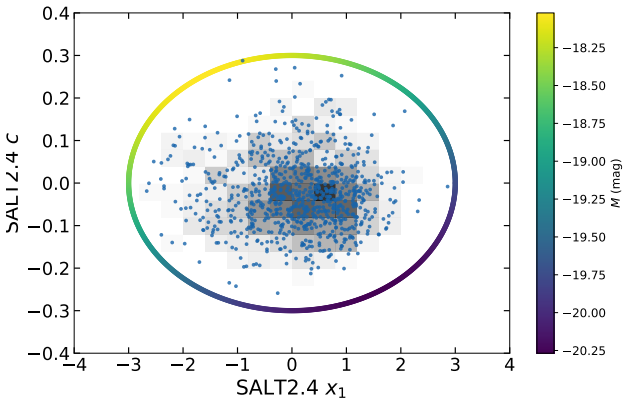

Fig. 1. SALT2.4 stretch and color lightcurve parameters of SNeIa from the SDSS, PS1 and SNLS samples from the pantheon catalog. The individual SN data are shown as blue dots and a 2D histogram is shown in grey to highlight point density. The ellipse encapsulating all the SN data is displayed colored by the effective standardized absolute magnitude using the α and β standardisation coefficents from (Scolnic et al. 2018).

with major axis $x_1 = 3$ and manor axis $c = 0.3$ incapsulate the full distribution (see also **?**, for a similar contour but using a less conservative $c = 0.2$). Assuming the average SN absolute magnitude ($x_1 = 0$, $c = 0$) is $M = -19.36$ (**??**) we can derive the absolute magnitude of SNeIa along this ellipse given the standardisation coefficient from (**?**): $\alpha = 0.16$ and $\beta = 3.14$.

The faintest SNIa is that with $x_1 = -1.66$ and $c = 0.25$ and has an absolute standardized magnitude at peak in Bessel-b band of -18.31 mag, which leads to limiting asbolute magnitude of -18.00 if we want to be able to observe it typically a week before and 10 days after peak. Therefore, given the 5σ point source detection magnitude limit of a magnitude limited survey, one can derive the maximum redshift above which the faintest SNeIa will start to be missed.

SNLS typically acquires SNeIa in the redshift range $0.4 < z < 0.8$. At these redshifts the rest-frame Bessel-b band roughly corresponds to the SNLS-i filter, that has a 24.8 mag 5σ depth [1]. This converts to a $z_{lim} = 0.60$, in perfect agreement with (**?**) and (**?**). Similarly, PS1 observing SNeIa in the range $0.2 < z < 0.4$, their g-band 5σ depth is 23.1 mag (**?**), corresponding $z_{lim} = 0.30$. The fig. 6 of (Scolnic et al. 2018) suggests a more conservative z_{lim} of 0.27 for the PS1 catalog. In similar redshift range, SDSS has a limiting magnitude of 22.5 (**???**), which would lead to a $z_max = 0.24$. However, the SDSS survey were more sensitive to limited spectroscopic ressources. **?** presents that during year-1 of SDSS, SNeIa with $r - mag < 20.5$ where favored for spectroscopic follow up, corresponding to the redshift cut at 0.15. For the rest of the SDSS survey, additional spectroscopic ressources where used, such that **?** and **?** of show a relative completness up to $z_{lim} = 0.2$. For the rest of the analysis, we will use $z_{lim} = 0.2$ as baseline magnitude.

In Section **??**, we test the impact on using more conservative redshift limits ($z_{lim} = 0.15$ for SDSS, $z_{lim} = 0.27$ for PS and $z_{lim} = 0.55$ for SNLS, following Fig. 14 of **?**). The cuts on the raw data of those three samples are shown figure fig:cuts.

In addition, we use the SNe Ia sample of from the nearby supernovae factory (SNfactory **?**) published in (Rigault et al. 2018). As the SNe search were much deeper than the spectrophotometric follow-up, SNfactory SNe Ia within a redshift range of

[1] CFHT final release website.

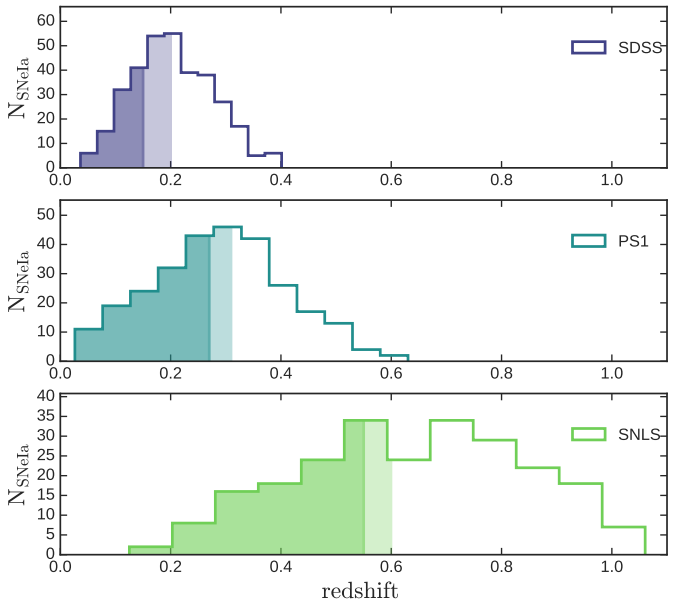

Fig. 2. Histograms of the 3 surveys on which we applied cuts to get rid of selection effects, as discussed in section 2.

Table 1. Origin of the SNeIa in our sample and redshift limit (if applicable) of each surveys.

Survey	N_{SN}	z_{lim}
SNf	141	–
SDSS	167	0.20
PS1	160	0.30
SNLS	102	0.60
HST	26	–

$0.02 < z < 0.09$ should also be a random sampling of the underlying SN population. The HST sample from Pantheon follows the same logic and we therefore kept it entirely (**?**).

Our "complete sample" is therefore made of 656 SNeIa whose composition is detailed in table 1.

CHECK LITERATURE CAN WE USE THE CfA SAMPLES ???

3. Method

We used the LsSFR and stretch measurments from the SNf sample. The LsSFR has an evolution with the redshift that is analytically known: calling the fraction of young stars and the fraction of old ones, Rigault 2018 et + find

$$\frac{\delta}{\psi} \equiv \text{LsSFR} = K \times 1 + z^{\varphi} \tag{1}$$

with = 2.8, and knowing + = 1:

$$\delta = K^{-1} \times 1 + z^{-} + 1^{-1} \tag{2}$$

$$\psi = K \times 1 + z^{+} + 1 \tag{3}$$

The goal is to find how the stretch depends on the LsSFR, distinguishing old and young SNe which fractions evolve with the redshift, in order to have an analytical law for the mean redshift evolution of the stretch. The measured data on which we

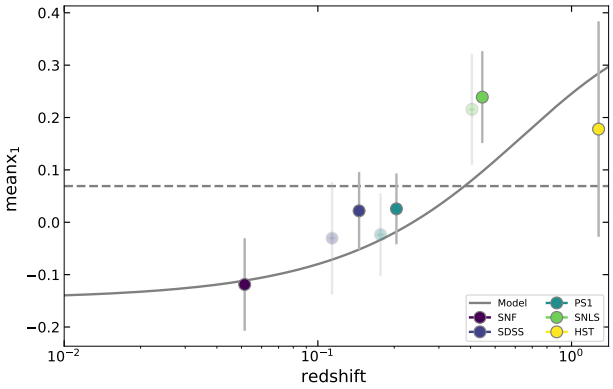

Fig. 3. Result of the model fitted on SNF data and mean of stretch and redshift of the other surveys used for this analysis. Conservative data is shown in transparent markers.

based our first model is plotted in figure **??**; based of the shape of the x_1 vs LsSFR cloud, we implemented the following model:

- **young**: a gaussian of mean $_1$ and standard deviation $_1$, namely $_1 \equiv {}_{1,1}$;
- **old**: a linear combination between $_1$ and another gaussian $_2 \equiv {}_{2,2}$

As such, the probability to observe a young SNe Ia labeled "i" with a stretch x_1^i and error $\dot{x}_1^i$ is

$$p x_1^i, \dot{x}_1{}^i|_{1,1} = {}_1, {}_1{}^2 + \dot{x}_1^{i\,2}(x_1^i) \tag{4}$$

and for an old one:

$$p(x_1^i, \dot{x}_1^i|_{1,2,1,2}, a) = a \times {}_1, \sqrt{{}_1{}^2 + \dot{x}_1^{i\,2}}(x_1^i) + (1-a) \times {}_2, \sqrt{{}_2{}^2 + \dot{x}_1^{i\,2}}(x_1^i), \tag{5}$$

where a is the relative amplitude between the two gaussians. Finally, the normalized stretch distribution at a given z $x_1|z$ is the weigthed sum of both young and old stretch distributions given their relative fraction :

$$x_1|z = \times_1 + 1 - \times a_1 + (1-a)_2 \tag{6}$$

We fitted it on SNf data, giving the results table 2, with a graphical representation shown figure 3. For clarity with the next models, we named it 3G2M2SSNf for it has a total of 3 gaussians but with only 2 means and 2 standard deviations, and has been fitted on SNf data only.

We implemented and compared 10 models in total, 4 of which have an evolution with the redshift from , and 6 don't (= f = cst). The ones with and evolution are:

- 3G2M2S, the one we described (but fitted on all the data);
- 3G2M1S, where this time $_1 \equiv {}_2$;
- 2G2M2S, model taken from HOWELL 2009 where we added ;
- 3G3M3S, with three independent gaussians.

The ones without a stretch evolution are the same ones but with an "F" implying we set = f = cst, and two others:

- 1G1M1S, where there is no distinction between old and young SNe;

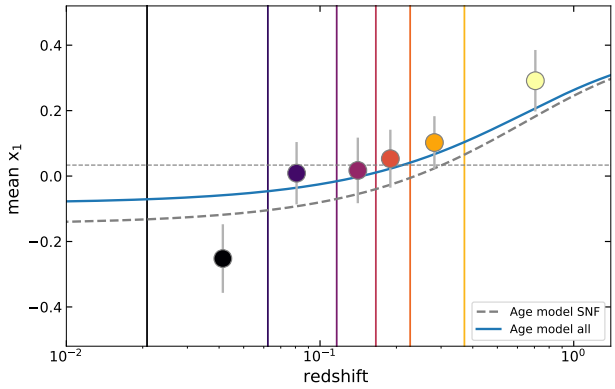

Fig. 4. Result of the model fitted on all surveys data cut at the non-conservative $z_{\max}$. We chose the bins to compute the means of stretch and redshift by making them equal in number of SNe Ia.

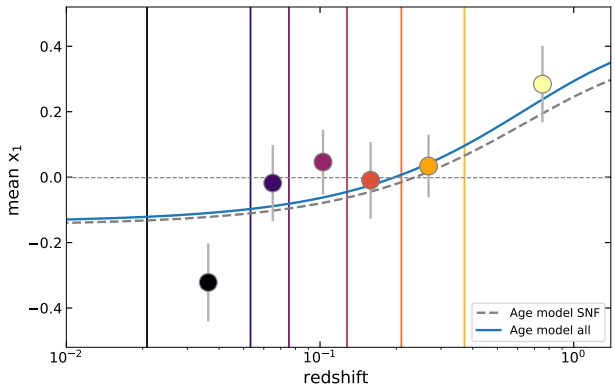

Fig. 5. Result of the model fitted on all surveys data cut at the conservative $z_{\max}$. We chose the bins to compute the means of stretch and redshift by making them equal in number of SNe Ia.

– 1G1M2S, taken from KESLLER 2017 and used in recent cosmological analysis SCOLNIC 2018. It's an asymetric model where

$$p(x_1^i, \mathrm{x}_1^i|_{,-},_{+}) = \begin{cases} \mathcal{N}, \sqrt{{}_{-}{}^2 + \mathrm{x}_1^{i\,2}}(x_1^i) & \text{if } x_1^i \geq \\ \mathcal{N}, \sqrt{{}_{+}{}^2 + \mathrm{x}_1^{i\,2}}(x_1^i), & \text{else} \end{cases} \quad (7)$$

The fitted parameters are showed table 2.

To test the coherence of this model, we also fitted it using all the data from the surveys indistinctly. These results are shown figures 5 and **??**

4. Results

To compare all these models, we use the Akaike Information Criterion corrected for sample size (BURNHAM 2002), that penalises the increase of free parameters in order to discourage overfitting:

$$\mathrm{AICc} = \mathrm{AIC} + 2kk + 1n - k - 1 \quad (8)$$

with $\mathrm{AIC} = 2k - 2\ln\mathcal{L}$, where k is the number of free parameters and the likelihood. The probability for a model to be as representative as the "best" one is given by:

$$p(\mathrm{other} > \mathrm{best}) = \exp \mathrm{AICc}/2 \quad (9)$$

The results are showed table 3. We find that every model lacking an evolution of the stretch with the redshift is systematically worse than those that implement it.

5. Conclusion

Stretch evolution with the redshift is a thing. Need to see if it has an impact on the cosmology though.

Acknowledgements. This project has received funding from the European Research Council (ERC) under the European Union's Horizon 2020 research and innovation programme (grant agreement n 759194 - USNAC). Support has been provided by the Institut Universitaire de France, the CNES, and the region Auvergne-Rhone-Alpes.

References

Abbott, T. M. C., Abdalla, F. B., Alarcon, A., et al. 2018, Phys. Rev. D, 98, 043526
Ata, M., Kitaura, F.-S., Chuang, C.-H., et al. 2017, MNRAS, 467, 3993
Chabanier, S., Millea, M., & Palanque-Delabrouille, N. 2019, MNRAS, 489, 2247
Coles, P., & Jones, B. 1991, MNRAS, 248, 1
Freedman, W. L., Madore, B. F., Hatt, D., et al. 2019, ApJ, 882, 34
Jones, D. O., Riess, A. G., Scolnic, D. M., et al. 2018, ApJ, 867, 108
Knox, L., & Millea, M. 2019, arXiv e-prints, arXiv:1908.03663
Poulin, V., Smith, T. L., Karwal, T., et al. 2019, Phys. Rev. Lett., 122, 221301
Planck Collaboration, Aghanim, N., Akrami, Y., et al. 2018, arXiv e-prints, arXiv:1807.06209
Reid, M. J., Pesce, D. W., & Riess, A. G. 2019, arXiv e-prints, arXiv:1908.05625
Riess, A. G., Macri, L. M., Hoffmann, S. L., et al. 2016, ApJ, 826, 56
Riess, A. G., Casertano, S., Yuan, W., et al. 2019, ApJ, 876, 85
Rigault, M., Copin, Y., Aldering, G., et al. 2013, A&A, 560, A66
Rigault, M., Aldering, G., Kowalski, M., et al. 2015, ApJ, 802, 20
Rigault, M., Brinnel, V., Aldering, G., et al. 2018, arXiv:1806.03849
Scolnic, D. M., Jones, D. O., Rest, A., et al. 2018, ApJ, 859, 101
Wong, K. C., Suyu, S. H., Chen, G. C.-F., et al. 2019, arXiv e-prints, arXiv:1907.04869
Z

Table 2. Valeurs des paramètres pour différents modèles. En rouge les données aberrantes.

Model	a	f	$_1$	$_1$	$_2$	$_2$
$3G2M2S_{SNf}$	0.48 ± 0.07	none	0.39 ± 0.07	0.56 ± 0.05	-1.5 ± 0.1	0.52 ± 0.09
3G2M2S	0.48 ± 0.17	none	0.36 ± 0.08	0.61 ± 0.05	-1.3 ± 0.2	0.60 ± 0.12
3G2M2SF	0.1 ± 0.6	0.2 ± 0.6	-0.9 ± 0.7	0.7 ± 0.3	0.5 ± 0.2	0.6 ± 0.1
3G2M1S	0.47 ± 0.07	none	0.35 ± 0.04	0.61 ± 0.03	-1.25 ± 0.10	$_1$
3G2M1SF	0.2 ± 0.9	0.7 ± 0.3	0.36 ± 0.04	0.60 ± 0.03	-1.23 ± 0.10	$_1$
2G2M2S	none	none	0.49 ± 0.04	0.54 ± 0.03	-0.72 ± 0.08	0.83 ± 0.07
2G2M2SF	none	0.3 ± 0.2	-0.9 ± 0.6	0.7 ± 0.2	0.5 ± 0.2	0.56 ± 0.09

Model		
1G1M1S	0.01 ± 0.04	0.90 ± 0.03

Model		$_-$	$_+$
1G1M2S	0.16617 ± 0.00004	1.07 ± 0.04	0.69 ± 0.03

Model	a	f	$_1$	$_1$	$_2$	$_2$	m_3	$_3$
3G3M3S	0.14 ± 0.08	none	0.51 ± 0.06	0.54 ± 0.04	-1.9 ± 0.2	0.29 ± 0.11	-0.55 ± 0.12	0.67 ± 0.15
3G3M3SF	0.2 ± 0.2	0.10 ± 0.04	-1.7 ± 0.2	0.4 ± 0.1	0.9 ± 0.1	0.3 ± 0.2	0.0 ± 0.2	0.7 ± 0.1

Table 3. Comparaison des modèles. NR représente les modèles implémentés durant ce stage. (F) indique les modèles pour lesquels il n'y a pas d'évolution de la fraction de SNe Ia jeunes et vieilles en fonction du redshift.

Name	Description	Free param	$\ln \mathcal{L}$	$AICc$	$AICc$	Proba
3G2M1S	NR 1S	4	1815	1823	0.0	1.0
3G2M2S	NR 2S	5	1815	1825	-2.0	3.6×10^{-1}
2G2M2S	Howell	4	1818	1826	-3.4	1.8×10^{-1}
3G3M3S	NR 3S	7	1812	1826	-3.6	1.6×10^{-1}
3G3M3SF	NR 3S (F)	8	1813	1829	-6.3	4.3×10^{-2}
2G2M2SF	Howell (F)	5	1823	1833	-9.9	7.0×10^{-3}
3G2M1SF	NR 1S (F)	5	1823	1833	-10.4	5.5×10^{-3}
3G2M2SF	NR 2S (F)	6	1823	1835	-12.0	2.5×10^{-3}
1G1M2S	Kessler (F)	3	1837	1843	-20.2	4.1×10^{-5}
1G1M1S	1 gauss. (F)	2	1872	1876	-53.5	2.4×10^{-12}